ANALYSIS OF AM-241 RESUSPENSION INTO ATMOSPHERE

A Major Qualifying Project
Presented to
The Academic Faculty

By

Paula Sarrion Silvestre

In Fulfillment
of the Requirements for the Bachelor's Degree
Department of Physics
Department of Mathematical Sciences

Worcester Polytechic Institute

May 2019

ANALYSIS OF AM-241 RESUSPENSION INTO ATMOSPHERE

Approved by:

Prof. David Medich
Department of Physics
Worcester Polytechnic Institute

Prof. Jian Zou
Department of Mathematical Sciences
Worcester Polytechnic Institute

Prof. Zhongqiang Zhang
Department of Mathematical Sciences
Worcester Polytechnic Institute

Date Approved: May 25, 2019

ACKNOWLEDGEMENTS

I would like to acknowledge and thank my advisors, Professors David Medich, Jian Zou and Zhongqiang Zhang, for their help and guidance throughout the completion of this Major Qualifying Project. I also want to thank Shaun Marshall for all his help, feedback and support.

TABLE OF CONTENTS

LIST OF FIGURES

ABSTRACT

In health physics, there is a need to model the resuspension of radiological particulates into the atmosphere to help evaluate radiological security thresholds. Previous studies have failed to reach an agreement on the proposed model. Therefore, this project is part of doctoral research that aims to experimentally measure resuspension and derive a mathematical model that fits the experimental results. Based on a compartment kinetic model, we successfully derived a theoretical exponential model that describes resuspension in a closed setting without environmental effects. Experimental set-up and procedures were determined to collect data from three different trials. The data collected didn't significantly measure resuspension due to an oversampling of the population. Revision of procedures will allow a successful measurement of resuspension that will be fit to the proposed model.

CHAPTER 1
INTRODUCTION

1.1 Purpose of the Project

The purpose of this project is to measure the resuspension into atmosphere of stable $Eu203$, which is a chemical analog of radioactive Am^{241}_{203}. This project will study the resuspension kinetics of two particle size groups (1-10um and 0.1-1um) on a concrete surface for an initial 100% surface deposition. These results will be compared against a theoretical kinetics model that assumes first-order particle transport between ground, surface, and air. These results will be used as the basis for future research to allow the incorporation of environmental conditions, such as wind, rain or temperature, into the calculation of more complex resuspension kinetics and population risk.

1.2 Resuspension

"Following the deposition of trace materials on soil surfaces, a frequent observation has been that airborne concentrations of that trace material occur over the contaminated soil surface" (Anspaugh et al., 2011). This process is known as resuspension.

The study of airborne resuspension has gained importance in many fields related to industrial processes and environmental applications (Alloul et al., 2002). In the health physics field, it has become essential to find an accurate resuspension model for radiological materials into atmosphere, because they can be inhaled or ingested resulting in a dangerous or prejudicial dose pathway for certain radionuclides (Anspaugh et al., 2011). Furthermore, knowledge of resuspension models can help evaluate and develop specific procedures and radiological security thresholds (Marshall, 2018).

For a hypothetical accident scenario or controlled experiment, resuspension coefficients are used to calculate the amount of radiological material that would be redispersed into the immediate

environment or settling onto the ground. The resuspension coefficient is important, therefore, to asses radiological consequences of depositions, accidents or other processes, and to determine the necessary protection and measures to follow.

Due to its importance, analysis of resuspension following a nuclear accident and for controlled experiments have been conducted for the past sixty years to predict the atmospheric concentration of particles after a mass release. As a consequence, several models and resuspension coefficients have been developed to try to fit the dependence of resuspension on different parameters like time, environmental effects or human alterations.

1.3 Historical Studies of resuspension

The study of resuspension began with the analysis of how sand is blown into atmosphere to form sand dunes and cause soil erosion (Anspaugh et al., 2011). These studies developed equations that explained the physics behind different scenarios under meteorological variables, however, resuspension played a minor role in these models.

The rise of nuclear weapons and concern about radiological accidents, brought focused interest back to particle resuspension. This topic became an important key in health physics and different experiments were performed to find an accurate model.

Following the advancement of nuclear weapons, Stewart (1964) performed measurements of particle resuspension and developed an equation for the rate at which particles resuspend into atmosphere (resuspension factor), K, as a factor of the measured air concentration "X" and the total area of deposition density "D" (m^{-2}):

$$K = S_f = \frac{X}{D} \tag{1.1}$$

During that time, two experiments: Project 56 and 57, were conducted at the Nevada Test Site. Specifically,Project 56 studied the dispersal of plutonium through four tests. While, Project 57 measured the deposition of plutonium much later on time. The result for the resuspension factor,

presented by Langham et al. (1955) was:

$$S_f(t) = 10^{-6} exp(\frac{-0.693t}{45\text{days}}) \tag{1.2}$$

Shreve (1958) fitted the data from Project 57 to a power function of time, $t^{-0.75}$. However, in 1968, Kathren proposed the following resuspension model for plutonium resuspension in soil:

$$S_f(t) = 10^{-4} exp(\frac{-0.693t}{35\text{days}}) \tag{1.3}$$

Based on Kathren's equation, Anspaugh et al. (1975) proposed a revised model:

$$S_f(t) = 10^{-4} exp(-0.15\sqrt{t} + 10^{-9}) \tag{1.4}$$

In 1999, the U.S National Council on Radiation Protection and Measurements (NCRP) based on measurements and studies of the Chernobyl accident recommended the following model :

$$S_f(t) = \begin{cases} 10^{-6} & \text{t} < 1\text{d} \\ \frac{10^{-6}}{t} & 1\text{d} < \text{t} < 1{,}000\text{d} \\ 10^{-9} & \text{t} > 1{,}000\text{d} \end{cases} \tag{1.5}$$

After a thorough study of different resuspension models, some of which have been described in this paper, Anspaugh and Maxwell presented in 2011 a new equation to describe the resuspension factor:

$$S_f(t) = 10^{-5} e^{-(8.10x10^{-7})t} + 7 * 10^{-9} e^{-(2.31x10^{-8})t} \tag{1.6}$$

Even though federal institutions and the health physics community use the 2011 model proposed by Maxwell and Anspaugh, the debate surrounding resuspension is still open. As can be seen in the differences in the selection of parameters, the effect of meteorological variables and the functions in the models presented above.

When it comes to meteorological variables, Stewart's (1964) resuspension factor has no dependence on environmental factors, but Shreve (1958) observed that wind speed had a clear effect on resuspension. On top of that, in Langham's (1971) model, time has a much stronger effect on the factor than any meteorological variables.

Furthermore, the resuspension factor equations vary from exponential to power functions without agreeing which function provides the best data fit. For example, Shreve's power function equation obtains a good data fit for the first data values, but a poor fit after 15 days (Anspaugh et al, 2011). Whereas, Maxwell and Anspaugh most recent proposed equation is an exponential function and it obtains a good data fit for $t<100$ (Anspaugh et al, 2011).

These resuspension models also differ in time dependence; as Stewart's equation has no time dependence while most of the other models do. Surprisingly, in other studies data has proven to be different from what theory would predict; Garland's (1982) observed resuspension at low wind speeds, when the theoretical prediction is that in such environment resuspension would not occur. However, Garland's observation might not representative of atmospheric resuspension as unidirectional wind speeds achieved in a wind tunnel are not representative of open environments (Anspaugh et al, 2011).

Over the past decades, controversy has been building up around resuspension. Anspaugh (2011) noted that this controversy arises from the lack of understanding of the process of resuspension of trace materials, which results in the lack of consensus in definition of resuspension factor. While the resuspension factor is understood to be the fractional quantity of airborne particles that arose from the surface, some studies include initially suspended particles prior to the deposition.

1.4 Project Goal

The controversy surrounding resuspension can be traced back to the definition of resuspension itself, as depending on how resuspension is understood the studied time frames will change and the data included in the study will be different. For our project we will understand resuspension as the fractional quantity of airborne particles that arose from the surface, not including those particles

that are still in fall-out.

The goal of this project is to measure resuspension in an experimental setting and derive a kinetic model for a compartment system that will give a good data fit for the experimental results. Both the model and the experiment will be looking at resuspension without any meteorological influences, as we believe that by finding a standard model for isolated resuspension we can create a foundation from which other experiments and models can be derived.

First we will design a system for the experiment that will allow us to study resuspension by collecting samples during a certain period of time. The samples will be analysed by Neutron Activation Analysis and we will obtain measurements of resuspension during specified time frames. While, the derived kinetic model will mirror the experiment to provide good data fits and theoretical estimates for resuspension over time.

CHAPTER 2

BACKGROUND

2.1 Kinetic Models

The catenary or compartment model, is a kinetic model that linearly connects each compartment to one or two of its neighbours. In this model, each i^{th} compartment trades particles with its neighboring compartments at rate constants: $k_i$and k_{-i}. As shown in figure 2.1:

$$\underset{k_{mig}}{\longleftarrow} \boxed{X_{\text{Surface}}} \underset{k_{dep}}{\overset{k_{res}}{\rightleftharpoons}} \boxed{X_{\text{Air}}} \underset{k_{dis}}{\longrightarrow}$$

Figure 2.1: General Caternary Model

These model can also be described as being open or closed, depending on the behaviours of the compartments situated at the edges of the system. If the edge compartments transfer particulates outside of the system, then it is open. But if the edge compartments (the right or leftmost compartments) only transfer particulates to the neighboring inner compartment, then the system is closed. Figure 2.2 illustrates the open and closed systems, respectively.

$$\underset{k_{mig}}{\longleftarrow} \boxed{X_{\text{Surface}}} \underset{k_{dep}}{\overset{k_{res}}{\rightleftharpoons}} \boxed{X_{\text{Air}}} \underset{k_{dis}}{\longrightarrow} \qquad \boxed{X_{\text{Surface}}} \underset{k_{dep}}{\overset{k_{res}}{\rightleftharpoons}} \boxed{X_{\text{Air}}}$$

Figure 2.2: Open and Closed Cartenary Model

In the following chapter, we will look into two compartment systems that mirror our experimental set-up and will derive each model in the search of a solution for the number of particles in air and the resuspension factor.

2.2 Neutron Generator

In this project, we use a neutron generator to analyse the experiment samples. The one that was available for our project operates using deuterium-deuterium fusion. In the generator, a high voltage electric field controls plasma, through which a deuterium beam is accelerated and aimed at a deuterium target. The deuterium ions produce fusion when they collide with the deuterium targets, as a result Helium-3 isotopes and neutrons are created. Due to the initial forward momentum of the ions, the neutrons tend to recoil forward (while some recoil in every direction) and are ejected through the front of the generator beam at an energy of 2.5 MeV. At this energy, the neutrons are considered "fast neutrons" and are unlikely to be absorbed by most materials. This beam therefore is moderated by slowing down the neutrons to thermal energy (approximately 0.025 eV) using elastic collisions with nuclei. Then, at this range the neutrons can now be used for neutron activation.

2.3 Neutron Activation Analysis

Neutron Activation Analysis, also referred as NAA, is a method widely used to perform quantitative and qualitative analysis of trace elements in experimental samples (Glascock, 2017). NAA consists of radiating samples with neutrons to measure the presence of tace elements in the sample (IAEA, 2016).

In this technique a sample is irradiated with neutrons, in our case using the neutron generator mentioned above. During the neutron exposure, some of the nuclei in the sample will absorb a neutron increasing its atomic number. As shown in figure 2.3, the nuclei will go back to a more steady configuration by releasing gamma rays.

The radioactive emissions detected by NAA provide valuable information about the neutrons density. Furthermore, the spectrum of these radioactive emissions can be studied to determine the composition of different particles in the sample. In the case of Eu-203, when a neutron beam is absorbed by a nucleus, the nucleus de-excites to the radioactive form of Eu-154. Then, Eu-154

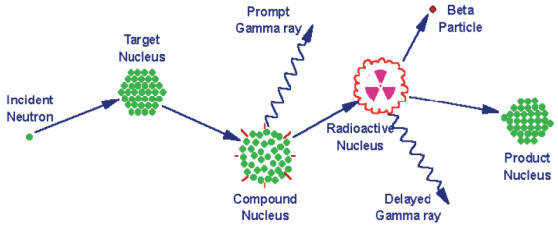

Figure 2.3: Diagram of nucleus life during NAA. (Glascock, 2017)

decays via emission of gamma rays that will be measured for intensity and energy.

To better understand what happens to the target nucleus, we will study the process in more detail. Suppose our sample has an initial population of N_0 stable target atoms. During the activation, the target atoms are irradiated with a uniform beam of mono-energetic neutrons with a specific fluent rate, ϕ. The number of atoms which absorb a neutron depends on three things: the exposure time, the beam intensity and the absorption cross-section of the nucleus. Specifically, the rate of neutron absorption, and therefore isotope generation is given as:

$$\dot{N} = \phi \dot{N}_0 \sigma \tag{2.1}$$

Where N is the number of activated isotopes at time t and σ is the cross section. Taking into account the radioactive decay of atom N, the number of atoms per unit of time is given as:

$$\frac{dN}{dt} = \dot{\phi} N_0 - \lambda N \tag{2.2}$$

Where λ is the decay constant of the isotopes, and λN is the number of isotopes that decay to a more stable nucleus (as seen in figure 2.3). Furthermore, for a mono-energetic beam of neutrons, we can assume that ϕ and N_0 do not have a dependence on time and can be understood as constants. Therefore, the term $\phi N \sigma$ can now be expressed as constant k. Also, we set our initial condition to be $N = 0$, as there are no prior daughter isotopes in the sample before its activation. Now we can

determine a general solution to the differential equation of the form:

$$N = k(1 - e^{-\lambda t}) \tag{2.3}$$

Then, we can define the number of activated isotopes as a function of time as:

$$N(t) = \frac{\dot{\phi} N_0 \sigma}{\lambda}(1 - e^{-\lambda t}) \tag{2.4}$$

The activity of the daughter isotopes can be found by multiplying the number of activated isotopes by the decay constant corresponding to the isotope:

$$A(t) = N_0 \sigma \phi (1 - e^{-\lambda t}) \tag{2.5}$$

Therefore, the gamma-rays of the irradiated sample can be measured to perform gamma spectroscopy on the sample, as the gamma-rays of daughter isotopes are characteristic of their parent nuclides, and the isotope's concentration in the sample can be determined.

2.4 Gold Foil Activation

During the NAA, the samples are activated together with gold foils of a small surface. The purpose of gold foil activation is to determine the flux that the sample is exposed to. By knowing the flux and the activity we can determine the number of atoms in the sample.

Gold is the element chosen for a different number of reasons, but mainly because it has a large neutron cross-section and a reasonably short half-life. Furthermore, gold only has one natural isotope (Au197) so it will only be excited to one state (Au198).

To determine the neutron beam flux, we will analyze through gamma spectroscopy the gamma rays emitted by the activated gold foil and record their energies and counts. Using a derivation of equation 2.6 and an equation for the number of counts of an activated sample (2.7), we can obtain an equation for the beam's flux.

Activity of sample:

$$A = N\sigma\phi Y(1 - e^{(} - \lambda t_i)) \tag{2.6}$$

Number of counts of an activated sample:

$$C = \epsilon \int A_0 e^{(} - \lambda t_d) e^{(} - \lambda t_c) \tag{2.7}$$

In these equations,N is number of target atoms, σ is the thermal neutron absorption cross-section, Φ is the neutron flux, λ is the activated species decay constant, Y is the fractional gamma yield for decay and t_i is the irradiation time.

It is also useful to introduce the relationship between the number of activated isotopes with Avogadro's number:

$$N_{Au} = (m_{Au} N_A)/(M_{Au}) \tag{2.8}$$

Combining equations 2.6, 2.7 and 2.8, we obtain a final equation for the thermal neutron flux determined by a known mass:

$$\phi = \frac{(C\lambda M_{Au})}{m_{Au} N_A \epsilon\sigma(1 - e^{-\lambda t_i}) e^{-\lambda t_d}(1 - e^{-\lambda t_c})} \tag{2.9}$$

Therefore, with every sample, we also activate a gold foil so we can determine the neutron beam flux and we can use the value to proceed with our resuspension calculations, as we will see in future chapters.

CHAPTER 3

METHODOLOGY

3.1 Kinetic Model

We consider the following linear model for all the three compartments.

$$\frac{d}{dt}\begin{pmatrix} X_a \\ X_s \\ X_g \end{pmatrix} = \begin{pmatrix} -K_{as} & K_{sa} & 0 \\ K_{as} & -K_{sa} - K_{sg} & K_{gs} \\ 0 & K_{sg} & -K_{gs} \end{pmatrix} \begin{pmatrix} X_a \\ X_s \\ X_g \end{pmatrix}. \tag{3.1}$$

Observe that $X_a + X_s + X_g = C$ is always a constant, independent of t as

$$\frac{d}{dt}(X_a + X_s + X_g) = 0.$$

From this observation, we reduce the linear system of 3 equations into a linear system of 2 equations. Here we consider $X_a,\ X_g$ only.

$$\frac{d}{dt}\begin{pmatrix} X_a \\ X_g \end{pmatrix} = K\begin{pmatrix} X_a \\ X_g \end{pmatrix} + \begin{pmatrix} 0 \\ CK_{sg} \end{pmatrix}, \quad K = \begin{pmatrix} -K_{as} & K_{sa} \\ -K_{sg} & -K_{sg} - K_{gs} \end{pmatrix}. \tag{3.2}$$

Moreover, we know that $X_a(0) + X_g(0) = C$ as $X_s(0) = 0$. The solution to the analytic form of X_a can be found in the Appendix.

3.2 Parameter estimation and simulation

Here we use the following approach to estimate the parameters in (3.2):

$$\min_{K_{as}>0, K_{sa}>0, K_{sg}>0, K_{gs}>0} \sum_{l=1}^{N} (X_a(t_l) - X_a^l)^2 \tag{3.3}$$

In this approach, we don't use any observations for X_g as we didn't collect any data for it. We only have the observations for X_a at time instants t_l, which are denoted as X_a^l.

In (3.3), we need to know the formulation of $X_a(t_l)$. We tried the following four forms to represent $X_a(t_l)$'s:

- Analytic formulation of $X_a(t_l)$ as the solution to (3.2) can be obtained explicitly. We present the analytic formulation in Appendix.

- Exponential integrator

$$\begin{pmatrix} X_a(t_l) \\ X_g(t_l) \end{pmatrix} = \exp(K(t_l - t_{l-1}))\left(\begin{pmatrix} X_a(t_{l-1}) \\ X_g(t_{l-1}) \end{pmatrix} + (t_l - t_{l-1}) \begin{pmatrix} 0 \\ CK_{sg} \end{pmatrix} \right) \tag{3.4}$$

- Mid-point scheme

$$\begin{aligned} \begin{pmatrix} X_a(t_l) \\ X_g(t_l) \end{pmatrix} &= (I - K(t_l - t_{l-1})/2)^{-1}(I + K(t_l - t_{l-1})/2) \begin{pmatrix} X_a(t_{l-1}) \\ X_g(t_{l-1}) \end{pmatrix} \\ &\quad + (t_l - t_{l-1})(I - K(t_l - t_{l-1})/2)^{-1} \begin{pmatrix} 0 \\ CK_{sg} \end{pmatrix}. \end{aligned} \tag{3.5}$$

- Backward Euler scheme

$$\begin{pmatrix} X_a(t_l) \\ X_g(t_l) \end{pmatrix} = (I - K(t_l - t_{l-1}))^{-1}\left(\begin{pmatrix} X_a(t_{l-1}) \\ X_g(t_{l-1}) \end{pmatrix} + (t_l - t_{l-1}) \begin{pmatrix} 0 \\ CK_{sg} \end{pmatrix} \right). \tag{3.6}$$

The next step is now to solve the minimization problem (3.3). We will use two approaches here.

The first approach is to find the derivatives of the object function with respect to the parameters to estimate and then let these derivatives be zero to derive the equations for these parameters. For

example, if we use the analytic formulation of X_a, we need the following derivatives

$$\frac{\partial}{\partial C_{k,j}} e^{\lambda_i t} = t e^{\lambda_i t} \partial_{C_{k,j}} \lambda_i, \quad \frac{\partial}{\partial C_{k,j}} \lambda_i e^{\lambda_i t} = (\lambda_i t + 1) e^{\lambda_i t} \partial_{C_{k,j}} \lambda_i. \tag{3.7}$$

We find this approach is not stable and rather cumbersome to find the equations for parameters. Hence we will not present the details here.

The second approach is to apply quasi-Newton methods to solve this problem. Quasi-Newton methods are used to find zeros or local maxima and minima functions in order to find roots or optimize the equation looked at. These methods are iterative, they involve a series of searches and computations of the function and its derivative at each iteration (Bonnars et al, 2006). A standard way to implement such methods is to use the MATLAB command fminunc (without constraints). The constrained problem (3.3) can be readily transformed to a problem without constraints by setting

$$K_{sa} = k_{sa}^2,\ K_{as} = k_{as}^2, K_{sg} = k_{sg}^2 \text{ and } K_{gs} = k_{gs}^2. \tag{3.8}$$

We now can perform the parameter estimation. The MATLAB code we use can be found in the Appendix.

Yet, there is another issue arising in the problem. The solution $(X_a, X_g)^\top$ are actually positive while only the exponential integrator and the analytic formulation can guarantee the positivitity of the solution when the values of the solution are close to zero. Thus, in the Euler scheme, mid-point scheme and the backward Euler scheme we take $(X_a, X_g)^\top = (|X_a|, |X_g|)^\top$ when they are very small.

Once we find the parameters through solving (3.3), we can run the model (3.2) to predict the values of $X_a(t)$ at unobserved time instants such as the values at future time instants.

For future studies, we will apply a Kalman filtering model to reduce the errors and noise in the

predictions. The Kalman Filtering problem (in discrete time) to solve would be,for $l = 0, 1, \ldots, N$,

$$\begin{aligned} \begin{pmatrix} Y_a^{l+1} \\ Y_g^{l+1} \end{pmatrix} &= (1 - K(t_{l+1} - t_l))^{-1} \begin{pmatrix} Y_a^{l} \\ Y_g^{l} \end{pmatrix} + \quad \text{“}Gaussian\, noise_1\text{”} \\ X_a^{l+1} &= BY_a^{l+1} + \quad \text{“}Gaussian\, noise_2\text{”} \end{aligned}$$

Here X_a^{l+1}'s are the observations/data collected from experiments and Y_a and Y_g are hidden but the correct model for X_A and X_G. The Gaussian noises will have zero means and to-be-determined covariances. Also, B as well as the parameters in K will be estimated using standard statistical techniques such as maximum likelihood estimation. A good reference for Kalman filtering is the book *Kalman Filtering: Theory and Practice Using MATLAB* by Angus P. Andrews and Mohinder S. Grewal.

As the noise is Gaussian, then Kalman filter minimizes the mean-square error of the estimated parameters. The algorithm can be described as a two-step process. The prediction step, in which the Kalman filter produces estimates of the current variables, along with their uncertainties. In the next step, after the outcome of the next measurement is observed, the given estimates are updated using a weighted average (Bishop and Welch, 2001).

By using Kalman Filtering in our proposed model, better results for parameter estimation will be obtained and the error from this calculations will be reduced.

3.3 Experiment

For the experimental study we designed a set-up that mirrors the kinetic models described above. This set-up allowed us to study resuspension of europium 203. This section describes the different steps and procedures of the experimental study of europium resuspension.

3.3.1 Materials

The materials used during the sample collection procedure are listed below:

- Europium, Eu2O3 powder, nanopowder (Dp $>$ 150 nm) (Sigma-Aldrich)
- Acrylic column tube, 4.25 in inner diameter, 6 ft high (US Plastic)
- Low-volume air sampling system, 2 Lpm (Atlantic Nuclear)
- 47 mm glass fiber filter, $99 - 97\%$ retention efficiency at Dp¡300 nm (Hach)
- Substrate material - Sand, soil, concrete, asphalt

We selected stable (non-radioactive) Eu203 because it is a chemical analog of Americium (an industrial radionuclide) which is a radioactive isotope of concern. As they are analogs, both Europium and Americium, have similar chemical and kinetic properties.

3.3.2 Experimental Setup

The experimental set-up follows the closed three-compartment kinetic model, creating a resuspension chamber that allows us to study the vertical resuspension of a deposited particle. We used concrete as a substrate material which was located at the bottom of the chamber and serves as the deposition surface for the Eu203 powder. The acrylic column tube works as the chamber wall that isolates the deposition from possible air currents or components in the experiment room. This set-up simulates the air concentration resulting from a large-scale (pseudo infinite) release. To measure the amount of particulates in the air compartment, the sampler head of the vacuum is located inside

the tube at a certain height (depending on the trial) and the vacuum pumps air through a 10ft long plastic tube up to the sampler head. The set-up is demonstrated in figure 3.1.

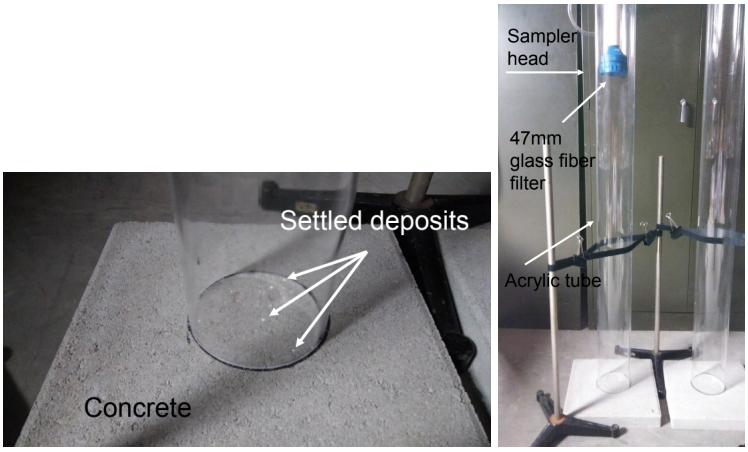

Figure 3.1: Experimental Setup

Then, 1g of Eu203 is deposited in each chamber by scooping the material into the concrete surface at the bottom of the chamber. We ran five concurrent experiments and analysed the results.

3.3.3 Trials and sampling procedures

During the course of the project, three different trials were carried through to obtain different sets of results and data that will help us reach conclusion on the resuspension of Eu_{203}.

Trial 1

For the first trial, the vacuum head was lowered to 0.25m from the concrete block surface with the objective of getting better readings from the samples. Following the deposition, without an initial waiting period, the air sampler was turned on. Over the four weeks of this trial, samples were collected on a daily basis, with the exception of some weekends when the lab could not be accessed. The air sampler was run for a predetermined time (24 hours) and the filters were retrieved from the sampler heads. The collected filters were placed in a sealed envelope and properly labeled (trial number, date and chamber number), and a new filter was placed in the sampler heads. The head is then moved back to its sampling location (0.25 m over the surface) and the air sampler was turned on.

Trial 2

For the second trial, the sampler head was also located at 0.25m from the surface. However, an initial waiting period of 3 days was allowed to compare the results with the previous trial and determine if the set-up was oversampling the particulates in the chamber. After the third day, samples were collected on a daily basis (including weekends) for two weeks. Again filters were exchanged and collected at the same two-hour interval and the system was put back to work.

Trial 3

For the last trial of this project, our aim was to obtain hourly rather than 24-hour long samples, to sample the particulate population rather than deplete the air chamber. The sampler head was located at 0.25m from the concrete surface and there was an initial waiting period of twenty-four hours. Then, filters were placed and the sampler system was be put to work for an hour. After sampling for one hour, the filters were collected and the air samplers were removed from the chamber. Twenty-four hours later, the filters and samplers were put back to work for another hour. Samples were taken over a period of two weeks.

3.3.4 Sample Activation

Once each experiment sequence was over, the samples were analyzed via NAA. The samples were activated using the neutron generator and measured with a Ge detector. In this project, the five samples that correspond to the same trial and time period are activated and analyzed together. The set of samples is activated together with a foil of gold, that is typed directly into the sample's envelope. As mentioned in the background, using the known mass of the gold foil we are able to calculate the neutron flux and therefore, use it to calculate the resuspension factor after analyzing the samples.

The samples and the gold foil are placed together in front of the beamline and blocked with solid water to increase neutron scatter, as it can be seen in Figure 3.2. After exposure to the neutron beam, the activated samples are placed directly on a Ge Detector to observe the decaying gamma rays of the sample over a period of 3-6 hours. From this point, we can study the gamma

spectroscopy to determine the presence of Eu2O3 in the sample using the results from the gold foil activation and other known variables extracted from the experiment. The results section will provide a detailed explanation of the analysis and the outcomes of the project.

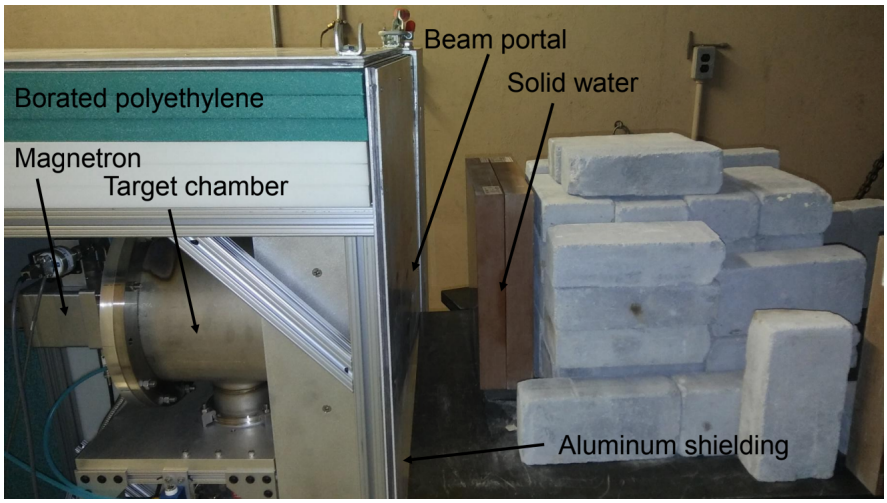

Figure 3.2: Neutron Generator

3.3.5 Expected Outcome

During the experiment, we predict that the powder deposited in the chamber will resuspend inside the chamber. Of the resuspended powder, a portion will stay on the surface of the chamber wall, while another portion will disperse in the air, travel by the air sampler and be collected when the powder impacts the filter in the sampler head.

After the samples are analyzed through Neutron Activation Analysis, we expect the calculations to give us four possible outcomes:

- No Eu content in the collection filter; which will point towards a dependence of lateral rather than vertical wind speed on resuspension.
- A negligible amount of Eu in the collection filter; this will require higher sensitivity probing and a revision of the set-up.
- A consistent baseline of resuspension. This is the desired outcome as this may indicate an accurate measurement of the background resuspension process.

- Unrealistically high concentrations, which may suggest an improper setup with the air sampler.

Our project has been designed and planned in a way that any alterations to the procedure or the set-up are simple and inexpensive to implement. Therefore, depending on the outcome of the trials we will be able to make the necessary adjustments and changes. The following section will provide in detail the project's outcomes and the decisions that were taken following the results.

CHAPTER 4

RESULTS

4.1 Experiment

4.1.1 Trial 1

Samples were taken over a period of four weeks and four daily samples taken. We used NAA to measure europium deposited daily from the first day up to the fourth. After the fifth sampling day, we could not detect any presence of europium in the sample.

As we can see in figure 4.1, the resuspension factor values for the first four days have a decreasing trend and, as mentioned above, there is no data after day four. All the values are within the same order of magnitude.

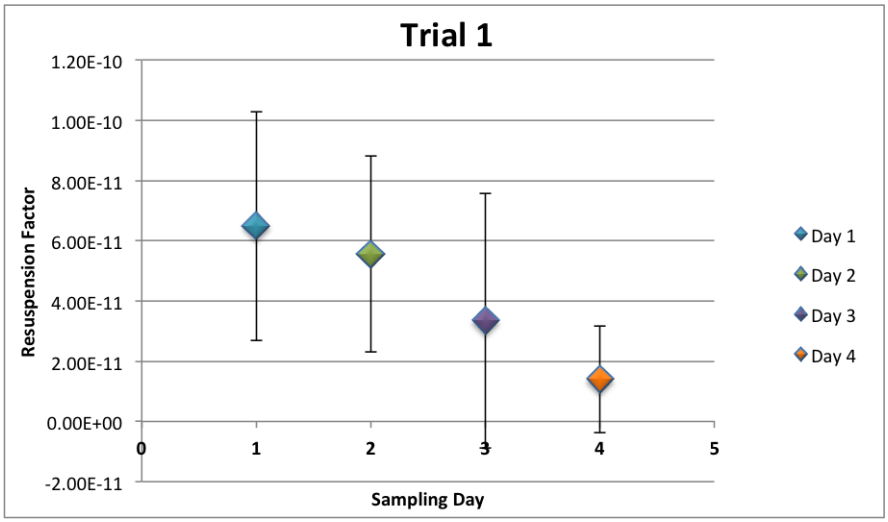

Figure 4.1: Trial 1: Daily Samples Resuspension Factor

Our aim was to obtain a consistent baseline for resuspension. However, during this trial we either obtained almost negligible amounts of Eu in the samples (first four days) and no Eu content (after day 4). These results point towards a revision in the sampling procedure and the set-up. Our hypothesis is that the air vacuum is oversampling to the point that after the fourth day the vacuum

had depleted the chamber. Due to this, we were not only measuring the resuspension but with each sample we were exhausting the Eu population in the chamber. This would explain the decreasing trend at earlier times than expected in the trial and the lack presence of Eu after the fourth day.

4.1.2 Trial 2

In Trial 2, we were looking to prove or discard the hypothesis that followed the results from trial one. Our aim was to compare the resuspension factor on the fourth and fifth days after deposition. Hence we had a 3 day waiting period before starting the daily (24-h) samples.

In figure 4.2 we can see the resuspension factors for the first two sampling days, that correspond to the fourth and fifth day after deposition. The resuspension factors are both in the same order of magnitude and still have a decreasing trend.

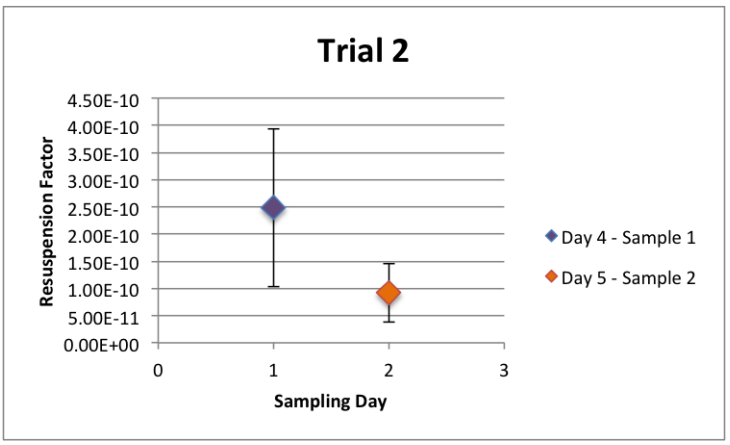

Figure 4.2: Trial 2: Daily Samples Resuspension Factor

In this trial, the lack of data after the fifth day does not mean that there was no presence of Eu on the following samples. No more samples could be analysed due to a problem with the neutron generator. There are two more weeks of data for this trial that are yet to be analysed.

However, the only two data points we obtained are sufficient to hold our hypothesis. The fact that in this trial we were able to measure the resuspension factor on the fifth day, together with the comparison in figure 4.3 help us notice that during the first sampling procedure we depleted the air chamber.

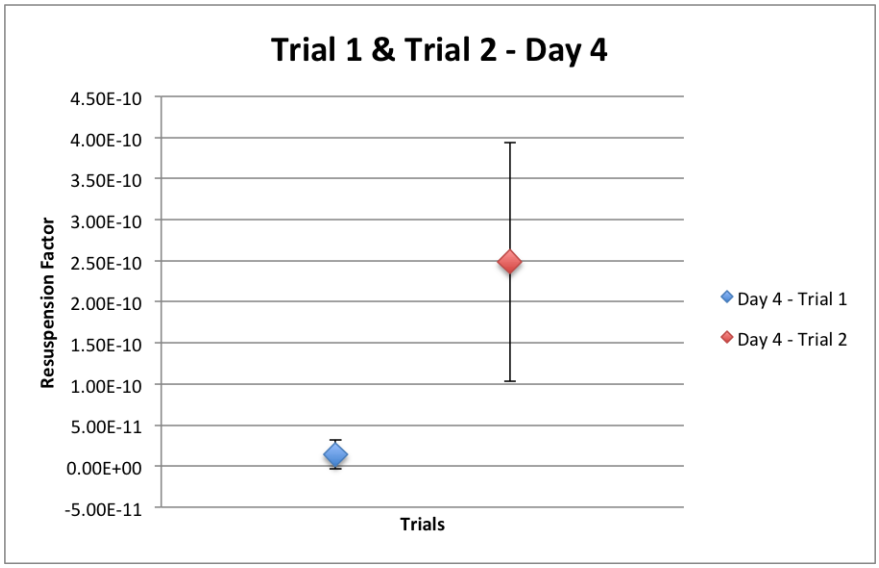

Figure 4.3: Day 4 resuspension factor, Trial 1 vs Trial 2

Both trials had the same set-ups, except from the initial waiting period. This leads us to think that the air vacuums are not sampling but eliminating the particulates from the chamber.

4.1.3 Trial 3

After the previous results, in trial 3 we kept the same experiment set-up but changed the sampling procedure. As mentioned in the methods section, we took hourly samples every day over a two-week period. Unfortunately, the neutron generator could not be fixed on time so we couldn't analyse this trial's samples.

4.2 Error Analysis

Due to the small amount of available data we are not able to perform a thorough statistical analysis of the results. However, from the available data we were able to estimate the error for each data point.

From the table below, we can see the resuspension factors corresponding to each sample day of the first and second trial.

Trial 1:

$$S_{f1} = \quad 6.49 * 10^{-11} \pm 3.8 * 10^{-11}$$

$$S_{f2} = \quad 5.56 * 10^{-11} \pm 3.25 * 10^{-11}$$

$$S_{f3} = \quad 3.35 * 10^{-11} \pm 4.23 * 10^{-11}$$

$$S_{f4} = \quad 1.40 * 10^{-11} \pm 1.77 * 10^{-11}$$

Trial 2:

$$S_{f1} = \quad 2.49 * 10^{-10} \pm 1.45 * 10^{-10}$$

$$S_{f2} = \quad 9.2 * 10^{-11} \pm 5.38 * 10^{-11}$$

From the data presented in the table and the graphs included in this section, the resuspension factors and the error are in the same order of magnitude, which means that the error higher than they should ideally be. On top of that, in most of the data points we are looking at an error of 60%. With these error, the values of resuspension factor vary a lot from the mean and indicate that our data is not a precise at it should be.

These error is calculated using error propagation for the resuspension factor equation, both equations are included in the appendix. Therefore, we can see how this error is related to all the calculations done prior to obtaining the resuspension factor such as the neutron activation analysis or the gamma spectroscopy. By reducing the error in the procedure and data analysis, we will be able to reduce the final error in the resuspension factor. Our goal is to present accurate measurements of resuspension for the development of security procedures and thresholds, hence we must aim to obtain errors around 1%.

4.3 Parameter Estimation and Prediction

In the last section, we described methods to solve the least squares problem (3.3). The first method, which consisted of deriving equation 3.7 was not successful in finding a solution as it was not stable. Therefore, we moved into the second method and tried the midpoint, exponential integrator and backward Euler techniques. We develop a MATLAB code to try out these techniques, the code is included in the appendix.

```
options = optimoptions('fminunc','MaxIterations',1e6,...
'OptimalityTolerance',1e-30);
k_solu_unc= fminunc(@(k)myfunc(xa_observ, k, t_observ,x0),...
k_guess,options);
```

Here the function 'myfunc' refers to the object function in (3.3). We take $k_{\text{guess}} > 0$ for the k's in (3.8) instead of for K_* . For the data presented in the last section, we use

$$K_{sa} = k_{sa}^2 = 0.0005,\ K_{as} = k_{as}^2 = 0.001, K_{sg} = k_{sg}^2 = 0.0005 \text{ and } K_{gs} = k_{gs}^2 = 0.001. \quad (4.1)$$

Observe the data are close to zero, we take absolute values of the numerical solution at each time step.

Of the three techniques, backward Euler was the most successful in estimating and predicting the parameters. Figure 4.4 shows the graphs for the estimation and prediction obtained by using Backward Euler in the MATLAB code.

For the parameter estimation, there were four parameters to estimate and the data points available for X_A. Then, we found values for the four rate constants and we looked into what values of X_A we could recover. The first graph in figure 4.4 shows the experimental values together with the recovered values.

The predicted values at several time instants from the model (3.2) using the estimated parameter are presented in the second graph of figure 4.4, which gives a trend that correlates with physical intuition, even though wiggles reflects some artifacts from preserving the positivity of X_A. Due to time constraints we were not able to apply Kalman filtering.

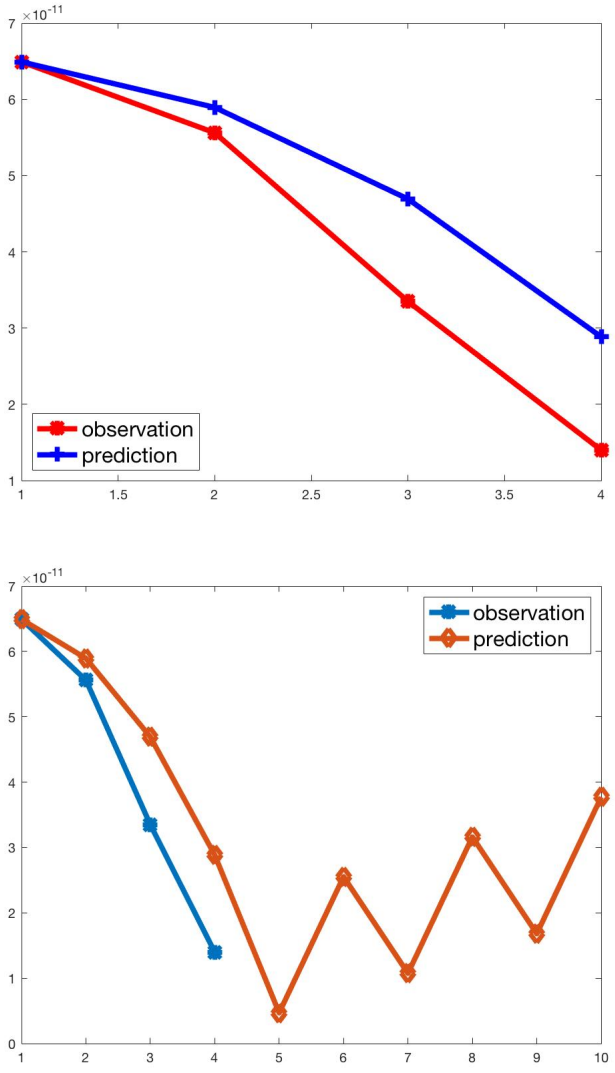

Figure 4.4: Parameter Estimation and Prediction

CHAPTER 5
DISCUSSION

5.1 Conclusion

There were four expected outcomes for this experiment, as we mentioned in the Background chapter. From the results presented in the previous chapter, we can group our findings into two outcomes:a negligible amount of Eu in the collection filter and no Eu content in the collection filter. In the previous section, it was determined that the lack of Eu content after the fourth day of sampling was caused by oversampling the particles in the chamber. Hence, these outcomes point towards a revision of the experimental set-up. As the probing might not be sensitive enough to detect Eu in the filters and the air vacuum should not be depleting the chambers.

It is also important to determine why the data from trial 1 differs from the one in trial 2 in almost two orders of magnitude, when the set-up and sampling procedure followed was the same for both trials. Similarly, the error estimate obtained for each data point was higher than desirable and it would be necessary to reduce it to have more accurate measurements of the resuspension factor. These two points bring us back to our experimental procedures, as they might be affecting the experiment's findings and precision. The collection and exchange of filters is a process than even when done carefully can cause the acrylic tube to move and the sampler head to hit the walls of the tube, which might alter the state of the particulates in the chamber and introducing more human error than we would like.

For the mathematical part of the project we were more successful than in the experiment section as we partially achieved our modeling goals. We were able to propose a model for resuspension based on the three compartment kinetic model and present an analytical solution for the air compartment. Even though the model proposed is a complex model and a highly non-linear system, we were able to develop a successful method to estimate parameters based on Quasi-newton and

Backward Euler methods. Due to the lack of experimental data, our work on parameter estimation and prediction was limited. Nonetheless, the results we obtained from the available data correlate with physical intuition and we built a foundation for future studies.

At the end of the day, the results obtained in this project may have not strictly measured the Eu resuspension in the sample. But the proposed model and the project will serve as a base for future work to refer back to, and a source of data and procedures that can be examined and improved. This project has defined a path to success for upcoming research and projects in resuspension.

5.2 Future Work

This project is the starting point for related projects to follow. Luckily, this project was part of an on-going doctoral research that will continue with the research based on our findings. Therefore, before starting again with more data collection the set-up must be reviewed to find a more sensitive, but less aggressive, air samplers. While also changing the chamber set-up to be more stable and less affected by any perturbation during the filter exchange process.

Once the neutron generator, gets back to work it would be really interesting and useful to analyse the samples left from Trial 2 to check if the chamber is depleted again from oversampling and to analyse Trial 3. The results from Trial 3 will help determine if the hourly sampling procedure works better than the daily procedure, these results would also help plan the next steps for the research.

The lack of experimental data and the time constraints of the project, affected our possibility of doing a more extensive work on parameter estimation. Here are some possible future directions of exploration on numerical methods once more reliable data are collected:

- Test whether the initial guess is proper as the quasi-Newton methods can only find local minimums instead of the global one.
- Test the presented approach is robust for various datasets.
- Repeat all the numerical tests in this chapter and compare them in performance.

- Apply a Kalman filtering model to accommodate the noise in the noisy data and to reduce the errors and noise in the predictions.

Keeping these recommendations in mind, we believe that this research could successfully measure a consistent baseline of resuspension, and it will be possible to fit the data to the compartment kinetic model. Hopefully, the future research is able to present a new and more accurate model for measuring and predicting resuspension.

Appendices

APPENDIX A

THE ANALYTIC FORM OF $X_A(T)$

The solution to the problem (3.2) can be written as follows.

$$\begin{pmatrix} X_a \\ X_g \end{pmatrix} = \exp(At) \begin{pmatrix} X_a(0) \\ X_g(0) \end{pmatrix} + \int_0^t \exp(A(t-s)) \begin{pmatrix} 0 \\ CK_{sg} \end{pmatrix} ds \tag{A.1}$$

Here $K = \begin{pmatrix} -K_{as} & K_{sa} \\ -K_{sg} & -K_{sg} - K_{gs} \end{pmatrix} = V\Lambda V^{-1}$, where Λ is the matrix of eigenvalues of A and V is the matrix of corresponding eigenfunctions.

Denote

$$C_{11} = -K_{as}, \quad C_{12} = K_{sa} \quad C_{21} = -K_{sg}, \quad C_{22} = -K_{sg} - K_{gs}. \tag{A.2}$$

Then $V = (V_1, V_2) = \begin{pmatrix} \lambda_1 - C_{22} & \lambda_2 - C_{22} \\ C_{21} & C_{21} \end{pmatrix}$, and the inverse matrix of V is

$$V^{-1} = \frac{1}{\det(V)} \begin{pmatrix} C_{21} & -(\lambda_2 - C_{22}) \\ -C_{21} & \lambda_1 - C_{22} \end{pmatrix}, \tag{A.3}$$

where

$$\det(V) = (\lambda_1 - C_{22})C_{21} - C_{21}(\lambda_2 - C_{22}) = C_{21}(\lambda_1 - \lambda_2). \tag{A.4}$$

Here the eigenvalues are

$$\lambda_1 = \frac{T}{2} + \sqrt{\frac{T^2}{2} - D}, \quad \lambda_2 = \frac{T}{2} - \sqrt{\frac{T^2}{2} - D}, \tag{A.5}$$

where

$$T = C_{11} + C_{22}, \quad \text{and} D = C_{11}C_{22} - C_{12}C_{21}. \tag{A.6}$$

The solution to (3.2) can be then written as follows.

$$\begin{aligned}
\begin{pmatrix} X_a \\ X_g \end{pmatrix} &= V\exp(\Lambda t)V^{-1}\begin{pmatrix} X_a(0) \\ X_g(0) \end{pmatrix} + \int_0^t V\exp(\Lambda(t-s))V^{-1}\begin{pmatrix} 0 \\ CK_{sg} \end{pmatrix} ds \\
&= V\exp(\Lambda t)V^{-1}\begin{pmatrix} X_a(0) \\ X_g(0) \end{pmatrix} + V\Lambda^{-1}(\exp(\Lambda t) - I)V^{-1}\begin{pmatrix} 0 \\ CK_{sg} \end{pmatrix}
\end{aligned} \tag{A.7}$$

A.0.1 Simplification of the formula

Let E be a diagonal matrix. Then by (A.3) and (A.4), we have

$$\begin{aligned}
& VEV^{-1} \\
= & \frac{1}{\det(V)}\begin{pmatrix} \lambda_1 - C_{22} & \lambda_2 - C_{22} \\ C_{21} & C_{21} \end{pmatrix} E \begin{pmatrix} C_{21} & -(\lambda_2 - C_{22}) \\ -C_{21} & \lambda_1 - C_{22} \end{pmatrix} \\
= & \frac{1}{\det(V)}\begin{pmatrix} (\lambda_1 - C_{22})E_{11} & (\lambda_2 - C_{22})E_{22} \\ C_{21}E_{11} & C_{21}E_{22} \end{pmatrix} \begin{pmatrix} C_{21} & -(\lambda_2 - C_{22}) \\ -C_{21} & \lambda_1 - C_{22} \end{pmatrix} \\
= & \frac{1}{\det(V)}\begin{pmatrix} (\lambda_1 - C_{22})D_{11}C_{21} - C_{21}(\lambda_2 - C_{22})E_{22} & (\lambda_1 - C_{22})(\lambda_2 - C_{22})(E_{22} - E_{11}) \\ C_{21}^2(E_{11} - E_{22}) & C_{21}E_{22}(\lambda_1 - C_{22}) - C_{21}E_{11}(\lambda_2 - C_{22}) \end{pmatrix}
\end{aligned}$$

From here and the solution of the form (A.7), we have

$$\begin{aligned}
X_a(t) &= \frac{1}{\det(V)}\big((\lambda_1 - C_{22})e^{\lambda_1 t}C_{21} - C_{21}(\lambda_2 - C_{22})e^{\lambda_2 t}\big)X_a(0) \\
&\quad + \frac{1}{\det(V)}(\lambda_1 - C_{22})(\lambda_2 - C_{22})(e^{\lambda_2 t} - e^{\lambda_1 t})X_g(0) \\
&\quad + \frac{C}{\det(V)}(\lambda_1 - C_{22})(\lambda_2 - C_{22})(\frac{e^{\lambda_2 t} - 1}{\lambda_2} - \frac{e^{\lambda_1 t} - 1}{\lambda_1})K_{sg},
\end{aligned} \tag{A.8}$$

and

$$\begin{aligned} X_g(t) &= \frac{1}{\det(V)} C_{21}^2 (e^{\lambda_1 t} - e^{\lambda_2 t}) X_a(0) \\ &\quad + \frac{1}{\det(V)} \big(C_{21} e^{\lambda_2 t} (\lambda_1 - C_{22}) - C_{21} e^{\lambda_1 t} (\lambda_2 - C_{22}) \big) X_g(0) \\ &\quad + \frac{CK_{sg}}{\det(V)} \big(C_{21} \frac{e^{\lambda_2 t} - 1}{\lambda_2} (\lambda_1 - C_{22}) - C_{21} \frac{e^{\lambda_1 t} - 1}{\lambda_1} (\lambda_2 - C_{22}) \big) \end{aligned} \tag{A.9}$$

Observe that $\lambda_1 \lambda_2 = D$ and $\lambda_1 + \lambda_2 = T$, where D and T are defined in (A.6).

$$\begin{aligned} (\lambda_1 - C_{22})(\lambda_2 - C_{22}) &= \lambda_1 \lambda_2 - C_{22}(\lambda_2 + \lambda_1) + C_{22}^2 \\ &= D - C_{22} T + C_{22}^2 \\ &= C_{11} C_{22} - C_{12} C_{21} - C_{22}(C_{11} + C_{22}) + C_{22}^2 \\ &= -C_{12} C_{21}. \end{aligned}$$

Then the solution (A.8) can be further simplified as

$$\begin{aligned} X_a(t) &= \frac{1}{\lambda_1 - \lambda_2} \big((\lambda_1 - C_{22}) e^{\lambda_1 t} - (\lambda_2 - C_{22}) e^{\lambda_2 t} \big) X_a(0) \\ &\quad - \frac{C_{12}}{\lambda_1 - \lambda_2} (e^{\lambda_2 t} - e^{\lambda_1 t}) X_g(0) \\ &\quad - \frac{CC_{12}}{\lambda_1 - \lambda_2} (\frac{e^{\lambda_2 t} - 1}{\lambda_2} - \frac{e^{\lambda_1 t} - 1}{\lambda_1}) K_{sg}, \end{aligned} \tag{A.10}$$

or in an equivalent form

$$\begin{aligned} X_a(t) &= \frac{1}{\lambda_1 - \lambda_2} \big((C_{11} - \lambda_2) e^{\lambda_1 t} - (C_{11} - \lambda_1) e^{\lambda_2 t} \big) X_a(0) \\ &\quad - \frac{C_{12}}{\lambda_1 - \lambda_2} (e^{\lambda_2 t} - e^{\lambda_1 t}) X_g(0) \\ &\quad + \frac{CC_{12}C_{21}}{\lambda_1 - \lambda_2} (\frac{e^{\lambda_2 t} - 1}{\lambda_2} - \frac{e^{\lambda_1 t} - 1}{\lambda_1}), \end{aligned} \tag{A.11}$$

or in an equivalent form

$$\begin{aligned} X_a(t) &= \frac{\lambda_1 e^{\lambda_1 t} - \lambda_2 e^{\lambda_2 t}}{\lambda_1 - \lambda_2} X_a(0) + \frac{C_{22} X_a(0) - C_{12} X_g(0)}{\lambda_1 - \lambda_2} (e^{\lambda_2 t} - e^{\lambda_1 t}) \\ &\quad + \frac{C C_{12} C_{21}}{\lambda_1 - \lambda_2} \left(\frac{e^{\lambda_2 t} - 1}{\lambda_2} - \frac{e^{\lambda_1 t} - 1}{\lambda_1} \right). \end{aligned} \tag{A.12}$$

This form of solution be further simplified using the facts $\lambda_1 \lambda_2 = D$ and $\lambda_1 + \lambda_2 = T$.

The solution (A.9) can be simplified as

$$\begin{aligned} X_g(t) &= \frac{C_{21}}{\lambda_1 - \lambda_2} (e^{\lambda_1 t} - e^{\lambda_2 t}) X_a(0) \\ &\quad + \frac{1}{\lambda_1 - \lambda_2} \big(e^{\lambda_2 t} (\lambda_1 - C_{22}) - e^{\lambda_1 t} (\lambda_2 - C_{22}) \big) X_g(0) \\ &\quad + \frac{C K_{sg}}{\lambda_1 - \lambda_2} \big(\frac{e^{\lambda_2 t} - 1}{\lambda_2} (\lambda_1 - C_{22}) - \frac{e^{\lambda_1 t} - 1}{\lambda_1} (\lambda_2 - C_{22}) \big). \end{aligned} \tag{A.13}$$

APPENDIX B

ESTIMATION AND PREDICTION CODE

This Appendix includes the MATLAB code used for the prediction and estimation of parameters mentioned in the Methodology and Results chapters.

Main Code:

```
clear
clc
close all

global scale_x
% Solve the minimization    problem

 scale_x =1e11;%e9;
 scale_t = 1;

% Now use the experimental data
t_observ =scale_t* [];
xa_observ = [];
xa_perturb =  [];

x0= [xa_observ(1); 0;1-xa_observ(1)];
x0= scale_x*x0;

xa_observ = scale_x*xa_observ;
xa_perturb = scale_x*xa_perturb;
```

```
pertub_level = 0.5;
xa_observ_p = xa_observ+  pertub_level*xa_perturb;

k_guess= [];
k_guess= sqrt(k_guess);

%% unconstraint
tic
options = optimoptions('fminunc','MaxIterations',1e6,...
    'OptimalityTolerance',1e-30);

k_solu_unc= fminunc(@(k)myfunc(xa_observ_p, k, t_observ,x0),...
    k_guess,options);
toc

k_solu= k_solu_unc.^2;
disp (k_solu )

%% parameter estimation

% Recover xa values for estimation
xa_recover = xa_exa(k_solu_unc , x0,t_observ) ;
% Plot estimated and observed parameters
figure (10)
plot([1 2 3 4], xa_observ/scale_x,'*-r', 'linewidth',4,'Markersize',10);
hold on
```

```
plot([1 2 3 4], xa_recover/scale_x,'+-b', 'linewidth',4,'Markersize',10);
hold off

legend('observation','prediction','Location','SouthWest','fontsize',16);

%% parameter prediction

% Predict xa values
t =scale_t*(1:10);
xa_predict = xa_exa(k_solu_unc , x0 ,t ) ;

% Plot predicted and observed parameters
figure(100)
plot(1:4, xa_observ/scale_x,'*-', 'Markersize',10,'linewidth',4);
hold on
plot(t,xa_predict/scale_x,'d-', 'Markersize',10, 'linewidth',4);
hold off
legend('observation','prediction','Location','NorthEast', 'fontsize',16);
```

Functions:

```
function    f=  myfunc(xa_observ, k, t_observ,x0)
%input
% --- k  = [k1, k2, k3,k4];
N= length(xa_observ);
M= length(t_observ);
if N~=M

    error()
```

```
end
xa_exact =xa_exa(k, x0,t_observ);
f = sum ((xa_observ-xa_exact).^2);

function    f=  myconstraint(k)

 k>0;

function xa_exact =xa_exa(k, x0,t_obs)

 % Recover Xa values
 % Input: k values from experimental data, initial x values, time

 K_mat =zeros(2,2);
 k =k.^2;
 K_mat(1,1) = -k(1);    K_mat(1,2) = k(2);
 K_mat(2,1) = -k(3);    K_mat(2,2) = -k(3)-k(4);

 deltat = diff(t_obs);
 nsteps= length(deltat);

 x_exact = zeros(2,nsteps+1);
 x_exact(:,1) = [x0(1); x0(2)];

 C = x0(1)+x0(2)+x0(3);  % total particles


f= [0;  C*k(3)];
```

```
for ii=1:nsteps
    x_exact(:,ii+1) =  exp(deltat(ii)*K_mat)*(x_exact(:,ii)+deltat(ii)*f);
    x_exact(:,ii+1) =abs(x_exact(:,ii+1));
end

xa_exact  = x_exact(1,:).';
```

APPENDIX C

PARAMETER EQUATIONS FOR RESUSPENSION FACTOR

The resuspension factor Sf and minimum detectable resuspension factor Sf are given below in terms of the 151Eu(n,) 152Eu reaction, the Eu2O3 compound, and other outlined experimental procedures (Eqs. C.1 and C.2).

$$MDS_f = \frac{A(k^2 + 2k\sqrt{2\mu_b})(M_{Eu-151} + \frac{M_{Eu-153}a_{Eu-153}}{a_{Eu-153}})}{\epsilon_F Y_{Eu} m_0 X_F f t_s \epsilon N_A \sigma_{Eu}(1 - e^{-\lambda t})(\frac{e^{-\lambda t}}{\lambda})(1 - e^{-\lambda \Delta t})} \tag{C.1}$$

$$S_f = \frac{AC^*(M_{Eu-151} + \frac{M_{Eu-153}a_{Eu-153}}{a_{Eu-153}})}{\epsilon_F Y_{Eu} m_0 X_F f t_s \epsilon N_A \sigma_{Eu}(1 - e^{-\lambda t})(\frac{e^{-\lambda t}}{\lambda})(1 - e^{-\lambda \Delta t})} \tag{C.2}$$

$$\phi = \frac{(C^{Au} M_{Au})}{m_{Au} N_A \epsilon \theta (1 - e^{-\lambda t_i}) e^{-\lambda t_d} (1 - e^{-\lambda t_c})} \tag{C.3}$$

The values listed in Figure C.1 will be obtained during the experimental calibration and procedure. Figure 2.6 list the physical properties and assumed parameters used in the experiments

through neutron activation analysis in the experiments of this study.

Parameter	Description
μ_b	(s^{-1}); Average detector background count rate
ϵ	Total detector efficiency for gamma spectroscopy
C^*	Count of gamma events from irradiated sample
m_{Au}	Mass of goil foil used for flux callibration
C^{Au}	Count of gamma events from irradiated gold foil
ϕ	(neutrons cm^{-2} s^{-1}); Neutron flux delivered to samples
t	(hr); time delay between activation and gamma detection
Δt	(hr); gamma detection time period

Figure C.1: Experimental values to be obtained during the procedure governing S_f and MDS_f through neutron activation analysis in the experiments of this study

Parameter	Value	Description
k	1.645	k-value of 95% confidence of non-Type I and II errors
Y_{Eu}	0.1420	Average yield of 841.6 keV γ from ^{151}Eu(n,γ)^{152}Eu
Y_{Au}	0.1420	Average yield of 841.6 keV γ from ^{197}Au(n,γ)^{198}Au
σ_{Eu}	3.30×10^{-21}	(cm^2); absorbtion cross-section of ^{151}Eu(n,γ)^{152}Eu
σ_{Au}	3.30×10^{-21}	(cm^2); absorbtion cross-section of ^{197}Au(n,γ)^{198}Au
N_A	6.022×10^{23}	(mol^{-1}); Avogadro's number- number of atoms in a mole
M_{Eu-151}	150.9	(g mol^{-1}); Molar mass of Eu-151
M_{Eu-153}	152.9	(g mol^{-1}); Molar mass of Eu-153
M_{Au}	152.9	(g mol^{-1}); Molar mass of Au-197
a_{Eu-151}	0.4791	Relative abundance of of Eu-151
a_{Eu-151}	0.5219	Relative abundance of of Eu-153
λ	0.0746	(hr^{-1}); decay constant for Eu-152
λ_{Au}	0.0746	(hr^{-1}); decay constant for Au-198
t_s	[1, 24, 168]	(hr); air sampling time period
τ	[2, 8, 24]	(hr); neutron irradiation time period
m_0	[0.010, 1.00]	(g); mass of initial compound deposition
X_F	0.70	Relative fraction of Eu to Eu_2O_3 by mass
A	9.152×10^{-3}	(m^2); surface area of deposition
f	3.333×10^{-5}	(m^3 s^{-1}); flow rate of air sampler
ϵ_F	0.99	Fiberglass filter partiulate capture efficiency

Figure C.2: Physical constants and assumed parameters governing S_f and MDS_f through neutron activation analysis in the experiments of this study.

REFERENCES

[1] L. H.R. A. Alloul L. Witschger O. and M. J., "Studies on the airborne resuspension of radioactive particle contamination," *Scientific and Technical Report 2002*, pp. 83–91, 1988.

[2] Anspaugh Lynn R. and Maxwell Reed M., "An Improved Model For Prediction of Resuspension," *Health Physics Society*, 2011.

[3] P. P.K. N. Anspaugh LR Shinn JH, "Resuspension and redistribution of plutonium in soils.," *Health Physics Society*, 1975.

[4] G. JA., "Resuspension of particulate matter from grass.," *Experimental programme 1979 –1980.*, 1982.

[5] S. T. Langham WH Harris PS, "Plutonium hazards created by accidental or experimental low-order detonation of atomic weapons.," 1955.

[6] L. WH., "Plutonium distribution as a problem in environmental science.," *Proceedings of environmental plutonium symposium.*, 1971.

[7] M. D. Marshall S. Potter C., "Reassesment of resuspension factor following radionuclide dispersal: Toward a general-purpose rate constant," *Health Physics Society*, 2018.

[8] N. C. on Radiation Protection and Measurements., "Recommended screening limits for contaminated surface soil and review of factors relevant to site-specific studies.," *Report No. 129*, 1999.

[9] S. J. Jr., "Operation plumbbob—preliminary report.," *Summary report, Test Group 57*, 1958.

[10] S. K., "The resuspension of particulate material from surfaces.," 1964.

[11] J. E. Turner, "Atoms, radiation, and radiation protection," 2007.

[12] C. L.C.A. S. J. F. Bonnans J. Ch.Gilbert, "Numerical optimization, theoretical and numerical aspects.," 2006.

[13] H. B.O. B. Skaflestad, "B-series and order conditions for exponential integrators," 2005.

[14] J. C. Butcher, "Numerical methods for ordinary differential equations," 2003.

[15] G. Welch and G. Bishop, "An introduction to the kalman filter," 2001.